

Title	Helicopter Location and Tracking using Seismometer Recordings
Creators	Eibl, Eva P. S. and Lokmer, Ivan and Bean, Christopher J. and Akerlie, Eggert
Date	2017
Citation	Eibl, Eva P. S. and Lokmer, Ivan and Bean, Christopher J. and Akerlie, Eggert (2017) Helicopter Location and Tracking using Seismometer Recordings. Geophysical Journal International, 209 (2). pp. 901-908.
URL	https://dair.dias.ie/id/eprint/382/

Helicopter Location and Tracking Using Seismometer Recordings

Abbreviated title: Helicopter Tracking Using Seismometers

I. AUTHORS, CONTACT INFORMATION

Eva P. S. Eibl^{1,2,*} (eva.eibl@ucdconnect.ie), Ivan Lokmer¹, Christopher J. Bean², Eggert Akerlie³

1: School of Earth Sciences, University College Dublin, Belfield, Dublin 4, Ireland

2: Geophysics Section, School of Cosmic Physics, Dublin Institute for Advanced Studies, 5 Merrion Square, Dublin 2, Ireland

3: Thyrluthjónustan ehf, Helo, Morkinni 3, 108 Reykjavik, Iceland now at: Nordurflug Helicopter Tours, Building 313, Reykjavik Domestic Airport, Reykjavik 101, Iceland

II. HISTORY DATES

Accepted date: XXX

Received date: June 2016

in original form date: XXX

III. CORRESPONDING AUTHOR

Eva P. S. Eibl

Geophysics Section, School of Cosmic Physics

Dublin Institute for Advanced Studies

5 Merrion Square, Dublin 2, Ireland

e-mail: eva.eibl@ucdconnect.ie

IV. SUMMARY

We use frequency domain methods usually applied to volcanic tremor to analyse ground based seismic recordings of a helicopter. We preclude misinterpretations of tremor sources and show alternative applications of our seismological methods. On a volcano, the seismic source can consist of repeating, closely spaced, small earthquakes. Interestingly, similar signals are generated by helicopters, due to repeating pressure pulses from the rotor blades. In both cases the seismic signals are continuous and referred to as tremor. As frequency gliding is in this case merely caused by the Doppler effect, not a change in the source, we can use its shape to deduce properties of the helicopter and its flight path. We show in this analysis that the number of rotor blades, rotor revolutions per minute (RPM), helicopter speed, flight direction, altitude and location can be deduced from seismometer recordings. Access to GPS determined flight path data from the helicopter offers us a robust way to test our location method.

V. KEYWORDS

acoustic signal, airborne object, Doppler effect, Fourier analysis, frequency gliding, tremor

VI. INTRODUCTION

The acoustic signal generated by a helicopter appears as repeating closely spaced pressure pulses caused by the rotation of the rotor blades (Eibl et al., 2015; Malovrh & Gandhi, 2005; Hardin & Lamkin, 1986). This type of signal (from moving objects) was reported in various studies on acoustic sensors (Kam & Ferguson, 2000; Damarla, 2010; Kalkan & Baykal, 2009; Nishie & Akagi, 2013; Oh & Lee, 2014). As a moving source passes a stationary receiver the recording shows a Doppler shift (Feynman, 2010). The frequency shift along with the angle information deduced from radar (Kalkan & Baykal, 2009) or microphones oriented in different directions (Damarla, 2010) was successfully used to estimate location, heading and altitude of the moving object.

Seismologists working on volcanoes usually encounter tremor accompanying eruptions (McNutt, 1992; Soosalu et al., 2005). Time and frequency domain methods are usually applied in order to analyse the temporal evolution of the signal. Location methods include arrival time based methods using the seismic envelopes of the signal (e.g. Lomax et al. (2000)), amplitude based location methods (e.g. in Eibl et al. (2014)) and array processing (e.g. Capon (1969)).

Due to the analogy of natural tremor, the helicopter-generated tremor can be recorded and analysed using seismological tools and techniques. Similarities and differences of volcano and helicopter related seismic tremor are highlighted in Eibl et al. (2015). Here, we expand this study and use a seismic array composed of seven seismometers in order to deduce rotor revolutions per minute (RPM), number of blades, speed, flight direction, altitude and approximate location of a helicopter. Whenever we refer to "altitude" in this study it is measured above the ground surface unless otherwise specified.

This exercise is a good example of how the same signal processing techniques can be used for solving different problems. It also emphasizes the non-unique problem of the signal generation. The same time and spectral features can be produced by different processes. For example, spectral glides can be produced by (i) a helicopter as a moving object (ii) a natural tremor source as a stationary object whose spectrum highlights the temporal changes in the source process. In this work, we address the case of a helicopter as a moving object.

VII. EXPERIMENTAL SETUP AND HELICOPTER TRACK

We recorded the seismic signal of a helicopter at a seven station broadband array with an aperture of 1.6 km in Jökulheimar, Iceland (Fig. 1). Stations have an elevation of 682.7 to 739.2 m a.s.l. and were installed to record flood and volcano seismic tremor (Eibl et al., 2017). The interstation spacing is

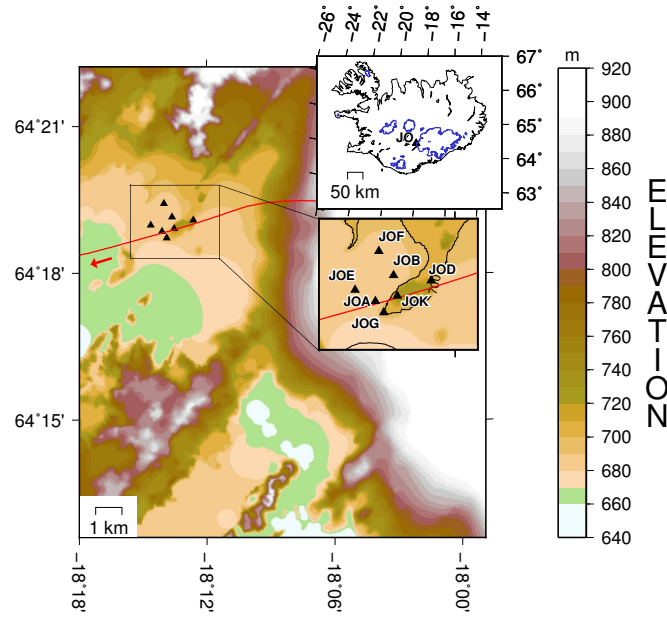


Figure 1. Location and geometry of the permanent seismic array in Jökulheimar, Iceland consisting of seven seismometers. The red line marks the flight route of the helicopter on December 19th, 2014. Elevation is above sea level based on data from the National Land Survey of Iceland. The top inset shows the array with respect to the whole island with glacier rims marked in blue. The middle inset is a zoom to the array including station names.

close enough to record the helicopter related signal at all stations and far enough to observe arrival time differences.

We show the GPS track of a four-bladed helicopter (Bell 407GX Serial no. 54308) in Fig. 1 that crossed the array at 11:53:30 on December 19th, 2014 travelling in a westward direction. The GPS track is from a Garmin 795 at a sampling rate of 5 Hz, a horizontal accuracy of at least 2 m and a vertical of tens of meters in the 'smart sampling' mode. In this mode points are saved every 1 to 18 s in order to save memory and to still track changes in the propagation direction (heading).

The rotors RPM is fixed at 413 (6.883 Hz) according to the manufacturer. We used the GPS track to calculate a speed of 207.3 ± 2.7 km/h, a mean flight direction of $253.5 \pm 1.2^\circ$ from north and an altitude of 961.5 to 969.1 m above sea level directly above the seismometers. The helicopter was closest to JOA, JOK and JOD and therefore north of JOG and south of all other stations (see inset in Fig. 1). Subtracting the elevation of the stations and due to station elevation differences the helicopter was 221.3 to 286.4 m above the stations (see column 1 in table II).

VIII. HELICOPTER GENERATED TREMOR

A detailed description of the helicopter generated tremor is given in Eibl et al. (2015) and Damarla & Ufford (2008). We therefore only provide a short summary here. The helicopter rotor blades create closely (temporally) spaced, repeating pressure pulses that merge into tremor. The spacing of the pulses in the time domain, as visible in Figs. 2a and b, is equal to the inverse of the spacing between spectral lines in the

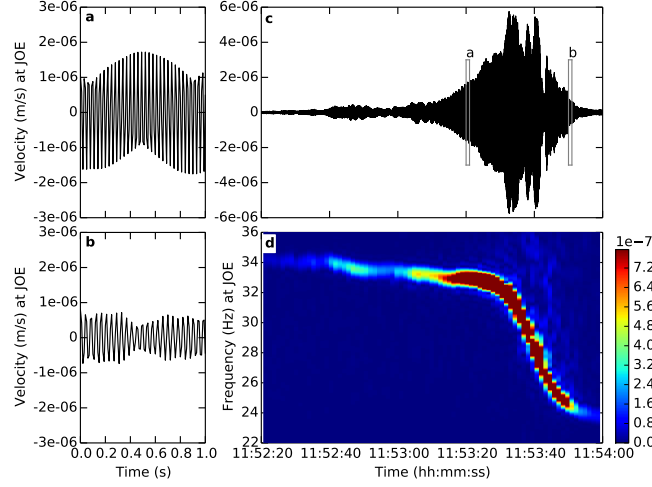


Figure 2. (a) 1 s long instrument corrected, vertical velocity seismogram of station JOE from 11:54:20, (b) same as subfigure a but from 11:54:50, (c) 100 s long instrument corrected, vertical velocity seismogram of station JOE during the flyby of the helicopter and (d) Amplitude spectrogram of the seismogram in c with a fast Fourier transform window length of 2 s. The characteristic shape of the curve is extracted at all stations (Fig. 4) and fitted in this study (Fig. 3).

frequency domain (see Eibl et al. (2015)). The central fundamental frequency of this tremor corresponds to the RPM times the number of rotor blades and is 27.53 Hz in our case. Due to the movement of the helicopter with respect to the stationary receivers the seismometers record a frequency up or down gliding caused by the Doppler effect (Fig. 2d or figs 2 and 5 in Eibl et al. (2015)). For the four-bladed helicopter we observed frequency gliding from 34 Hz down to 23 Hz within less than 40 s (Fig. 4).

IX. METHOD

A. The Shape of the Curve

When analysing the data in the frequency domain the shape of the gliding spectral curve can be described by:

$$f(t) = \frac{c \cdot f_s}{c + \frac{v_s^2 \cdot (t - t_0)}{\sqrt{v_s^2 \cdot (t - t_0)^2 + h^2}}} \quad (1)$$

for a source moving at constant speed along a straight line (e.g. Eibl et al. (2015)). $f(t)$ is the recorded frequency as a function of time t , c is the speed of sound (331.45 m/s at 0°C (Rienstra & Hirschberg, 2004)), f_s is the acoustic source frequency, v_s is the speed of the source and t_0 is the time of the closest approach (at distance h) between source and receiver. We can deduce information about the flight path of the helicopter from the characteristics of the curve: (i) minimum and maximum fundamental frequency (affected by the speed of the helicopter (see Fig. 3), (ii) the slope of the gliding (affected by the distance between source and receiver (see Fig. 3)), (iii) the time and frequency at the location of the inflection point. The observation (iii) corresponds to the time of closest approach and the frequency of the source, which can be directly determined (see Fig. 3).

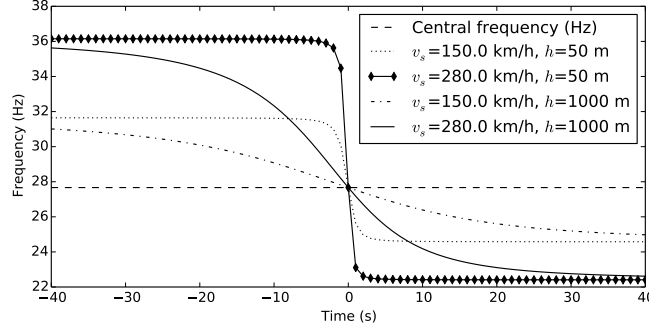


Figure 3. Sensitivity test of equation 1 using realistic values of v_s , f_s , t_0 and h . We show the curves for $f_s=27.668$ Hz, $c=331.45$ m/s (Rienstra & Hirschberg, 2004) and $t_0=0$. Respective curves for different f_s and t_0 are not shown, as changes do not affect the shape and mainly shift the curves with respect to the y or x axis, respectively. Note that the inflection point for each curve is at coordinate (f_s, t_0) , i.e. it corresponds to the source frequency and time of the closest approach for any choice of parameters at any station.

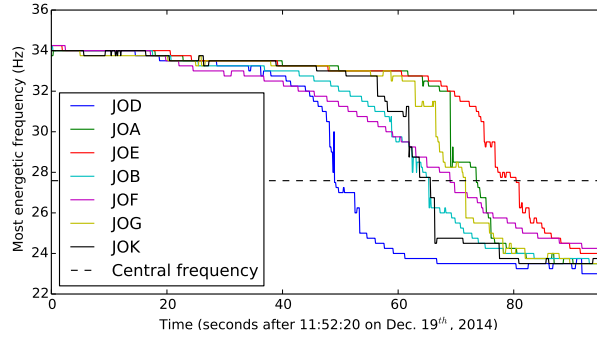


Figure 4. Extracted Doppler curves of a 100 s long time window of the vertical component of the stations in Jökulheimar. The frequency with maximum energy is picked in each spectrum (compare with Fig. 2d). Spectra are calculated for each 2 s long time window and for all seven stations.

t_0 does not have an effect on the shape of the curve and merely shifts it along the time axis. The true frequency of the source f_s is observed when the flight direction and source-receiver line segment are perpendicular - that is, at the time of the inflection point of the spectral curve. As with t_0 , f_s does not affect the shape of the curve, but a change would shift the entire curve along the frequency axis. Typical speeds range from 150 to 280 km/h (Eibl et al., 2015). Helicopter tremor can - depending on topography, wind direction and wind speed - be recorded at up to ~ 40000 m distance (see fig 5 and fig 7 in Eibl et al. (2015)). It is important to note that whilst even small changes in v_s strongly affect the minimum and maximum frequency, changes in h affect the steepness of the curve as visible in Fig. 3.

B. Curve Fitting With Four Unknowns

In order to perform a curve fit we analyse a 100 s long time window around the helicopter flyby. Spectra were calculated for 4 s long moving time windows with 97.7% overlap resulting in a good frequency resolution. We determine the most energetic frequency in each time window and create the frequency against time curve for each station (Fig. 4). These curves form the basis of our analysis.

We fit the recorded curve with equation 1 running the Levenberg-Marquardt algorithm (More, 1978) as

implemented in Beyreuther et al. (2010); Megies et al. (2011), in order to determine v_s , f_s , t_0 and h . However, after the first curve fit with four unknowns we realised that the minimum residual was still relatively large and that the plot of distance at closest approach against slope of the glide did not result in a smooth curve (see Fig. 6a). This indicated that the best fitting location derived from a curve fit with four unknowns was not correct as visible in Fig. 6b.

We realised that h along with v_s (see column 2 in table II) was systematically overestimated because the algorithm iterated to a local minimum for a curve fit with four unknowns. Different initial guesses did not improve the result. This can be avoided by exploring the entire 4-parameter space through a time consuming grid-search that will additionally reduce the residual.

C. Curve Fitting With One Unknown

In order to decrease the computational time and make the method capable of performing in 'real-time', we perform a curve fit with one unknown (h), a grid search over one unknown (v_s) and two fixed parameters (f_s , t_0) to explore the whole model parameter space. As f_s is the same for all stations, it does not affect the shape of the curve and can be directly derived from the inflection point, we fix f_s as mean of the f_s for each station as determined in the curve fit with four unknowns. Fixing f_s , t_0 can be directly determined from the inflection points of the best fitting curves with four unknowns (see Fig. 3). The speed from the curve fit with four unknowns serves as initial estimate for the next step. We perform a grid search over a range of source speeds v_s (in 1 km/h steps ± 30 km/h around the rough speed estimate), where we invert for h in the curve fit in each iteration, in order to find the values that result in the smallest residual (see column 3 in table II).

The curve fit of the whole curve is performed for each station i . In the next step the obtained parameters h , v_s , t_0 and f_s can be used to derive helicopter properties and its flight path (as detailed in sections IX-D, IX-E and IX-F).

Performing the curve fit with two unknowns t_0 and h , whilst doing a grid search over f_s and v_s , led to the same helicopter location.

D. Helicopter RPM and Number of Blades

Most helicopters (and all helicopters in Iceland) do not vary their main or tail Rotor RPM's during flight. The RPMs will only vary on take-off, landing and at low air speeds (Eurocopter, 2005; Robinson Helicopter Company, 1992).

In order to determine the RPM of the rotor blades we average f_s for all stations. As the RPM for helicopters in transit operated in Iceland is typically in the range of 375-415 RPM (6.25-6.917 Hz) (Eurocopter, 2005; Robinson Helicopter Company, 1992) the frequency f_s can be divided by this value

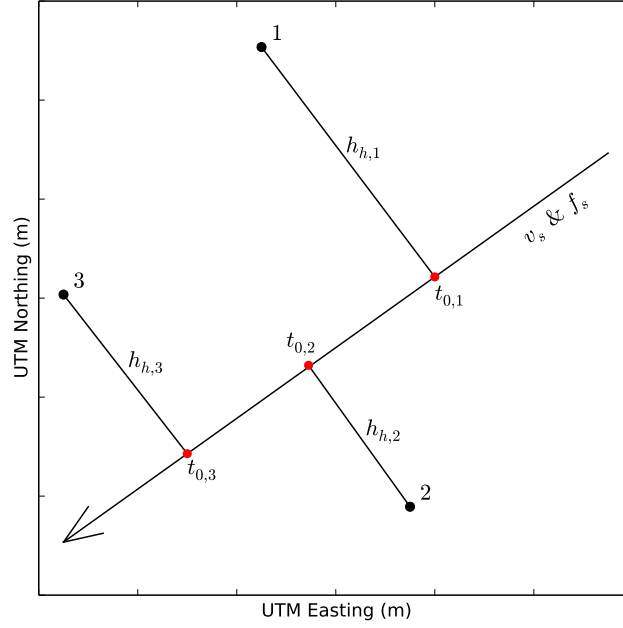


Figure 5. Schematic illustration of the parameters derived in the curve fit. They are used to locate the helicopter. Black dots mark stations i , red dots are projections of stations i on the helicopter flight track. Horizontal distances $h_{h,i}$ at times of closest approach $t_{0,i}$ are denoted as well as the global helicopter properties v_s and f_s . $t_{0,i}$ corresponds to the inflection points visible in Fig. 4.

to determine the number of rotor blades. If we then divide the frequency f_s converted to 1/min by the number of rotor blades rounded to the closest integer we can determine the actual RPM of the rotor blades.

Alternatively, it is possible to derive RPM, number of blades and speed of the helicopter directly from the minimum and maximum frequency (see equations 1 and 2 in Eibl et al. (2015)). However, deriving them from the whole curve is more robust.

E. Rough Flight Direction Estimate

In a next step we estimate the direction roughly based on arrival times. The time of the inflection points indicates the time when the helicopter is closest to each station i , thus representing observed arrival times $t_{0,i,obs}$ (Fig. 5). We draw an arbitrary flight direction line from 100 m north of the station where the signal arrived first and rotate it 360° in 0.5° steps. This starting point is chosen arbitrarily as the absolute helicopter location only plays a minor role when we determine a rough direction based on arrival times. For each angle, the seismometers are projected onto the line and residuals between the observed arrival times $t_{0,i,obs}$ and synthetic arrival times $t_{0,i,syn}$ were calculated (we know the speed of the helicopter). We systematically shift the arrival times so that the smallest arrival time in each case is 0 and estimate the

residual error R_1 based on

$$R_1 = 100 \cdot \sqrt{\frac{\sum_i (t_{0,i,syn} - t_{0,i,obs})^2}{\sum_i (t_{0,i,obs})^2}} \quad (2)$$

Then we exclude all directions for which the signal does not arrive first on the same station as observed in reality and pick the angle with the lowest error as a rough first estimate of the flight direction (see Fig. 7a).

For an exact direction determination, $t_{0,i,syn}$ needs to be corrected for the time the wave spends travelling through the air using $t_{0,i,syn} + \sqrt{h_{h,i}^2 + (h_{v,i} - h_{ar,i})^2}/c$, where $h_{h,i}$ is the horizontal distance, $h_{v,i}$ is the vertical distance and $h_{ar,i}$ corrects for elevation differences between the stations i . However, at this stage we do not estimate the altitude yet leading merely to a rough direction estimate. We recommend this step, as it is fast and avoids unnecessary iterations in the next, more time-consuming step.

F. Precise Helicopter Location

In order to estimate the location in the horizontal plane, altitude and exact flight direction we compare the observed distances $h_{obs,i}$ with theoretical distances $h_{syn,i}$ derived for various helicopter locations. We assume a flight route that is iteratively moved in 5 m steps between -1100 and +1200 m north-southwards of the station with the first arrival and in 10 m steps between 50 and 1000 m in altitude. The seismometer locations are again projected on the proposed flight route and horizontal distances to the stations at times of closest approach are calculated (see Fig. 5). The square root of the squared horizontal distances $h_{h,i}$ added to the squared assumed altitude $h_{v,i}$ are then compared to observed distances $h_{obs,i}$. A residual error R_2 was calculated as:

$$R_2 = 100 \cdot \sqrt{\frac{\sum_i (h_{syn,i} - h_{obs,i})^2}{\sum_i h_{obs,i}^2}} \quad (3)$$

with $h_{syn,i} = \sqrt{h_{h,i}^2 + (h_{v,i} - h_{ar,i})^2}$. We introduce the correction factor h_{ar} in order to correct the altitude for elevation differences of the stations.

We find the minimum in R_2 and repeat the procedure in 1° steps for directions $\pm 10^\circ$ around the best fitting flight direction. We then plot the minimum of R_2 for each direction against the flight directions (see Fig. 7c).

The minimum in the resulting residual R_2 (see Fig. 7b and c) reveals the flight direction, location and altitude of the helicopter when it passed the array. Plotting the distance of each station at the time of closest approach against the slope of the Doppler glide should trend towards -1 for small distances and towards 0 for larger distances as visible in Fig. 7d for our best fitting location.

Table I

OVERVIEW OF UNCERTAINTIES IN INPUT PARAMETERS (FREQUENCY, TIME OF CLOSEST APPROACH, SPEED OF THE HELICOPTER AND SPEED OF SOUND) AND OUTPUT PARAMETERS (DISTANCE OF CLOSEST APPROACH, DIRECTION, ALTITUDE AND HORIZONTAL LOCATION). UNCERTAINTIES OF THE INPUT PARAMETERS WERE PROPAGATED INTO THE DISTANCE AND FROM THERE INTO THE OTHER OUTPUT PARAMETERS.

	Data uncertainties: spectra/ grid search	Solution uncertainties: error propagated
RPM (1/min)	± 7.5	-
Time (s)	± 0.0454	-
Speed (km/h)	± 0.5	-
Distance (m)	-	4.0-9.7
Direction ($^{\circ}$)	-	± 3.5
Altitude (m)	-	± 25
Horizontal location (m)	-	± 95

G. Uncertainties

We give an overview of uncertainties of input and output parameters in table I. The length of the time window and overlap during the calculation of the spectra determines the time and frequency resolution of f_s and t_0 (see Fig. 4). We determine the uncertainty based on the resolution along the time and frequency axis. The uncertainty in time and frequency depend on each other i.e. a good time resolution requires a lower frequency resolution and vice versa. The uncertainty of v_s is based on the increments used in the grid search (column 1 in table I).

In a next step we determine the uncertainty in h by propagating the uncertainties of the input parameters using standard linear inversion theory. Finally, we estimate the uncertainty in the helicopter location and flight direction using the Monte Carlo method, where we vary the sets of input parameters within their uncertainty obtained in the previous step. The minimum and maximum values of these best fitting locations define the uncertainty given in column 2 in table I and in table II.

Underlying assumptions of our location method are that the source moves at constant speed along a straight line. We can however also see that there were slight changes in the speed and the direction during the flyby, which can introduce additional uncertainties. If the number of stations is sufficient this can be accounted for by using subsets of stations to derive altitude, location and directions at multiple times along the flight path.

X. RESULTS

A. Problems Around a Curve Fit With Four Unknowns

Initially we performed a curve fit with four unknown variables which are given in column 2 in table II. While RPM, direction and altitude seemed to be in agreement with GPS observations, the speed was

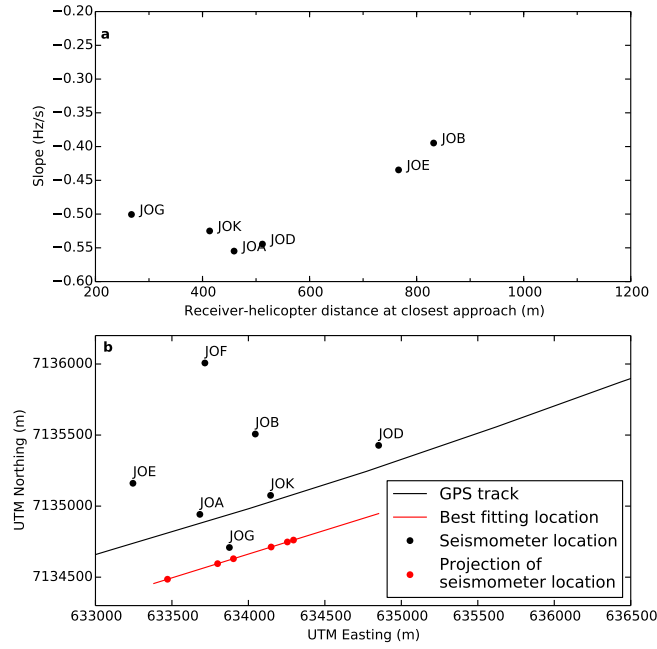


Figure 6. Helicopter location results as based on a curve fit with four unknowns. (a) Source-receiver distance at time of closest approach against the slope of the Doppler glide at the inflection points. (b) Best fitting helicopter location (red) in comparison to the helicopter GPS track (black). Red dots mark the station projection on the best fitting flight route.

overestimated by at least 10 km/h and the horizontal location was about 400 m too far south (see Fig. 6b). In addition the residual was relatively large. This is a consequence of overestimated speeds (5% corresponding to 10 km/h) and distances (24 to 67% corresponding to 80 to 740 m) in the curve fit with four unknowns. Performing a curve fit with speed and distance that both affect the shape of the curve, results in a local minimum that is in fact a compromise and not the best fitting curve.

We found that for three unknowns and increasing speed the frequency decreased. Lowering the speed and inverting for three, two or one unknown(s) in the curve fit led to a decrease of the distances to realistic values. Whilst a curve fit with four unknowns fitted the whole curve well, lowering the speed improved the fit during the glide but under-/ overestimated the starting/ ending frequency, respectively. This is reasonable as the gradual downwards gliding (see Fig. 2d) is caused by the gradual approach of the helicopter. For example at 11:52:20 it was still more than 2.8 km east of JOD and more than 4.4 km east of JOE. It is however subjective to determine by eye which part of the curve should be fitted for the best results. Therefore, we suggest searching iteratively over a variety of speeds in order to minimize R_2 .

B. Best Helicopter Location

In order to generally and objectively find the best fitting location of the helicopter we suggest performing a curve fit for four unknowns as a first step in order to get a rough parameter estimate for v_s and in order to determine f_s . As a second step, f_s should be fixed as mean of the f_s derived in the curve fit with four

unknowns and t_0 can be calculated. The distance of closest approach, h , is then obtained by the systematic grid search over a range of speeds, v_s , and the curve fit in the least square sense. Finally, the values of h for all stations are then used to determine the source (helicopter) location through a grid search for a location which minimises the sum of squared residuals between the calculated and observed values of h (R_2). This approach will decrease the residual R_2 in comparison to a curve fit with four unknowns.

For further objectivity, it is also possible to fix the source frequency and source speeds iteratively, whilst determining the times and distance at closest approach in a curve fit. This approach did not improve our location result further.

The helicopter location result with the smallest residual R_2 is shown in Fig. 7. The residual R_1 is given in Fig. 7a, the residual R_2 for the best fitting flight direction is shown in Fig. 7b and the minimum in R_2 for different directions is shown in Fig. 7c. A projection of the location with the smallest residual ($R_2=3.8$) with respect to the array stations and the GPS track of the helicopter is given in Fig. 7e. A good lateral fit is visible.

For the location with the lowest residual Fig. 7d shows the slopes of the gliding at the inflection points with respect to the distance of the station from the best fitting track as shown in 7e. The observed slopes converge to -1 for source-receiver distances approaching 0 m. For increasing distances slopes converge to 0. The visible linear trend supports our helicopter location.

Our analysis gives a RPM of 413.8 ± 7.5 for a four-bladed helicopter that flew at 212.0 ± 0.5 km/h towards $252.5 \pm 3.5^\circ$ at an altitude of 335.0 ± 25 m and was closest to JOA and JOK (see Fig. 7e and column 3 in table II). Our results are in accordance with the parameters derived from the GPS track as shown in table II apart from the altitude estimate.

We tested our code on another flyby of the same helicopter and could recover similar properties for a flight direction of about 67° using six available stations. However, as we do not have an exact GPS track and the helicopter passed south of all stations, we decided not to include it in this study.

C. Height Discrepancy

We have tested the sensitivity of our location method with respect to varying sound speeds and repeated it for sound speeds of 325.39 m/s, 331.45 m/s and 349.63 m/s at -10°C , 0°C and $+30^\circ\text{C}$, respectively. These changes did not affect the minimum residual, RPM and direction estimate. The effect on the horizontal location is merely 5 m and not systematic. However, we found systematic changes in helicopter speed and altitude. The higher the sound speed the higher is the estimated helicopter speed (212 to 222 km/h) and the lower is the altitude (335 to 320 m). Discrepancies between true and estimated helicopter speed and altitude might therefore be partly caused by wrong sound speed assumptions.

We have also compared the results of a grid search with a height resolution of 25 m to one with a height

Table II

COMPARISON OF PROPERTIES OF THE HELICOPTER AND ITS FLIGHT PATH DERIVED FROM THE GPS TRACK AND OUR SEISMOMETER RECORDINGS. WE SHOW RESULTS FOR A CURVE FIT WITH FOUR AND ONE UNKNOWN(S).

	GPS Derived Properties	Curve Fit 4 Unknowns	Curve Fit 1 Unknown
RPM (1/min)	4*413	4*(413.8 \pm 7.5)	4*(413.8 \pm 7.5)
Speed (km/h)	204.6-210.1	219.2 \pm 1.23	212 \pm 0.5
Direction ($^{\circ}$)	252.3-254.7	251.5 \pm 3.5	252.5 \pm 3.5
Altitude (m)	221.3-286.4	260.0 \pm 25.0	335.0 \pm 25.0
Closest to	JOA and JOK	JOG	JOA and JOK
Minimum R_2		22.8	3.8

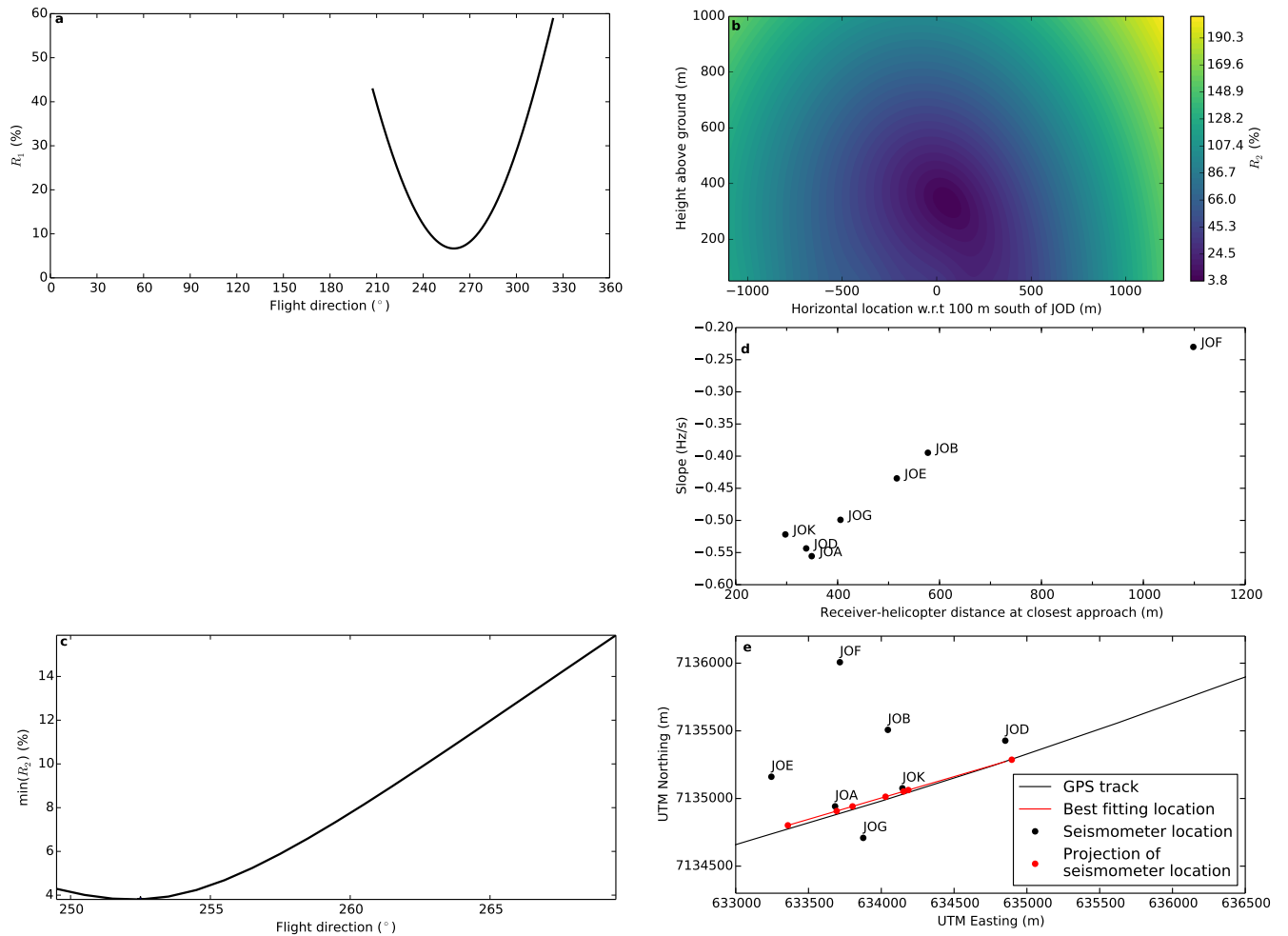


Figure 7. Helicopter location and residual errors based on the Doppler glides extracted from the vertical component of the stations in Jökulheimar. (a) R_1 of the rough flight direction estimation, (b) R_2 of the horizontal and altitude location at the best fitting flight direction, (c) Minimum of R_2 plotted against various flight directions, (d) Source-receiver distance at time of closest approach against the slope of the Doppler glide at the inflection points. (e) Best fitting helicopter location (red) in comparison to the helicopter GPS track (black). Red dots mark the station projection on the best fitting flight route.

resolution of 5 m. All other parameters were identical. In the run with a lower resolution the residual R_2 increased slightly but the overall location result was not affected: RPM, helicopter speed, direction and best fitting horizontal direction were identical. This indicates that the height is poorly constrained in our location method.

D. Gliding Spectral Lines in Volcano-Seismology and Glaciology

In volcano-seismology frequency gliding of volcanic tremor can have a few possible causes: (i) a change in the repetition time of a stationary source (Dmitrieva et al., 2013; Hotovec et al., 2013; Neuberg et al., 2000; Steel, 2009), (ii) a change in acoustic velocity (De Angelis & McNutt, 2007; Benoit & McNutt, 1997) or (iii) a change in dimension of the resonating body (De Angelis & McNutt, 2007; Jousset et al., 2003). Repeating processes such as frictional faulting (Dmitrieva et al., 2013; Hotovec et al., 2013; Lipovsky & Dunham, 2015), hybrid events (Neuberg et al., 2000) or merging low frequency events (Steel, 2009) are analogous to the helicopter generated tremor and are analogous to stick-slip motion between two adjacent icebergs (Talandier et al., 2006; MacAyeal et al., 2008) in glaciology.

Distinguishing if a frequency change is due to a lateral movement of the source as for helicopter generated tremor or a change in source repetition time as suggested for volcanic tremor is challenging. As mentioned in Eibl et al. (2015) the helicopter generated tremor shows strong frequency gliding if the helicopter is at a few kilometers distance and slower, less characteristic frequency gliding at larger distance. In volcano-seismology stations are usually at a larger distance from the source especially as the tremor source is below the Earth's surface. Therefore source changes would appear as gradual frequency changes, as often observed in the literature.

However, these gliding spectral lines are usually interpreted as changes in the temporal spacing between repeating pulses such as speeding up before explosions (source effect) rather than source movements (path dependent effect). It is possible to detect a source movement, if the shapes of the gliding spectral lines differ on different stations in a network or if they are time delayed with respect to each other. Network geometries that span various azimuths with respect to the tremor source are best suited to check for these path dependent differences of a moving source. On stations closer to the source a moving source might reveal a spectral curve shaped by the Doppler effect. Since a typical Doppler shaped curve can only be created by a moving source, this would be a strong indicator. Additionally, gaps in the tremor (e.g. Eibl et al. (2017)) or jumps in the fundamental frequency (Benoit & McNutt, 1997; Lesage et al., 2006; Hotovec et al., 2013) indicate a source effect of natural origin. Similarities and differences between volcanic and helicopter tremor as well as various not typical up- and downglidings were observed and discussed in Eibl et al. (2015) for helicopters at up to 40 km distance and in an experiment with acoustic sensors (Damarla & Ufford, 2008).

XI. CONCLUSION

In this study we use the recordings of seven seismometers (see Figs 2 and 4) arranged as array in Jökulheimar, Iceland (see Fig. 1) to track a helicopter (see Fig. 7e). We use seismological methods to derive properties of seismic tremor recordings in the frequency domain (see Fig. 4). These are used to perform a grid search (see Fig. 5) over direction, speed, altitude and horizontal location to find the values that best fit the observed arrival times and minimum source-receiver distances (see column 3 in table II). We present a method that can be used to deduce flight parameters of an airborne object such as a helicopter using merely seismometer recordings. We successfully deduced properties such as the number of rotor blades, RPM, speed, flight direction, location and altitude. Although precise spatial locations are only possible within the network, parameters such as the number of rotor blades, RPM, speed and flight direction can be determined as well for objects outside the seismic network. It is however necessary to have a source-receiver distance that allows for a Doppler glide in the recording. This cannot be observed if distances are too large allowing merely the determination of number of blades and their RPM (see fig. 7 in Eibl et al. (2015)).

We note that it was possible to improve the fit between the GPS track and best fitting location inverting for for example only one unknown (distance at the time of closest approach) in the curve fit and fixing speed, times of closest approach and frequency.

We show that the seismic tremor of a helicopter is generated by a repeating source process which is analogues to suggested tremor models in volcano-seismology and glaciology. However, in the case of a helicopter, frequency glidings are generated by the movement of the source, whereas in volcano-seismology and glaciology they are usually interpreted as a change in repeat time of a stationary source. We present a case study of location of a moving object using inversion of time-frequency transforms which can be of value to both academic and industrial communities with an interest in tracking airborne objects.

XII. ACKNOWLEDGMENT

The data were collected and analysed within the framework of FutureVolc, which has received funding from the European Union's Seventh Programme for research, technological development and demonstration under grant agreement No 308377. We thank two anonymous reviewers for constructive comments that helped to improve the manuscript and thank Matthias Vogt for advice on typical helicopter RPMs.

XIII. REFERENCES

Benoit, J. P. & McNutt, S. R., 1997. New constraints on source processes of volcanic tremor at Arenal Volcano, Costa Rica, using broadband seismic data, *Geophysical Research Letters*, **24**(4), 449.

- Beyreuther, M., Barsch, R., Krischer, L., Megies, T., Behr, Y., & Wassermann, J., 2010. ObsPy: A Python Toolbox for Seismology, *Seismological Research Letters*, **81**(3), 530–533.
- Capon, J., 1969. High-resolution frequency-wavenumber spectrum analysis, *Proceedings of the IEEE*, **57**(8), 1408–1418.
- Damarla, T., 2010. Azimuth & elevation estimation using acoustic array, in *Information Fusion (FUSION), 2010 13th Conference on*, pp. 1–7.
- Damarla, T. R. & Ufford, D., 2008. Helicopter detection using harmonics and seismic-acoustic coupling, *SPIE Proceedings*, **6963**.
- De Angelis, S. & McNutt, S. R., 2007. Observations of volcanic tremor during the January-February 2005 eruption of Mt. Veniaminof, Alaska, *Bulletin of Volcanology*, **69**(8), 927–940.
- Dmitrieva, K., Hotovec-Ellis, A. J., Prejean, S., & Dunham, E. M., 2013. Frictional-faulting model for harmonic tremor before Redoubt Volcano eruptions, *Nature Geoscience*, **6**(8), 652–656.
- Eibl, E. P. S., Bean, C. J., Vogfjörð, K., & Braiden, A., 2014. Persistent shallow background microseismicity on Hekla volcano, Iceland: A potential monitoring tool, *Journal of Volcanology and Geothermal Research*, **289**, 224–237.
- Eibl, E. P. S., Lokmer, I., Bean, C. J., Akerlie, E., & Vogfjörð, K. S., 2015. Helicopter vs. volcanic tremor: Characteristic features of seismic harmonic tremor on volcanoes, *Journal of Volcanology and Geothermal Research*, **304**, 108–117.
- Eibl, E. P. S., Bean, C. J., Vogfjörð, K. S., Ying, Y., Lokmer, I., Möllhoff, M., O’Brien, G., & Palsson, F., 2017. Silent Magma Flow Follows Tremor-rich shallow dyke formation: Bárðarbunga eruption, Iceland, *Nature Geoscience*, **in review**.
- Eurocopter, 2005. Flight Manual AS 350 B3 Arriel 2B1, Tech. rep.
- Feynman, R., 2010. *The Feynman lectures on physics.*, Reading, Mass: Addison-Wesley Pub. Co.
- Hardin, J. C. & Lamkin, S. L., 1986. Concepts for reduction of blade/vortex interaction noise, *Journal of Aircraft*, **24**(2), 120–125.
- Hotovec, A. J., Prejean, S. G., Vidale, J. E., & Gomberg, J., 2013. Strongly gliding harmonic tremor during the 2009 eruption of Redoubt Volcano, *Journal of Volcanology and Geothermal Research*, **259**, 89–99.
- Jousset, P., Neuberg, J., & Sturton, S., 2003. Modelling the time-dependent frequency content of low-frequency volcanic earthquakes, *Journal of Volcanology and Geothermal Research*, **128**(1-3), 201–223.
- Kalkan, Y. & Baykal, B., 2009. MIMO Radar Target Localization by Using Doppler Shift Measurement, *Proceedings of the 6th European Radar Conference*, (October), 489–492.
- Kam, W. L. O. & Ferguson, B. G., 2000. Broadband passive acoustic technique for target motion parameter

- estimation, *IEEE Transactions on Aerospace and Electronic Systems*, **36**(1), 163–175.
- Lesage, P., Mora, M. M., Alvarado, G. E., Pacheco, J., & Métaxian, J. P., 2006. Complex behavior and source model of the tremor at Arenal volcano, Costa Rica, *Journal of Volcanology and Geothermal Research*, **157**(1-3), 49–59.
- Lipovsky, B. P. & Dunham, E. M., 2015. Tremor during ice stream stick-slip, *The Cryosphere Discussions*, **9**(5), 5253–5289.
- Lomax, A., Virieux, J., Volant, P., & Berge-Thierry, C., 2000. *Probabilistic earthquake location in 3D and layered models - Introduction of a Metropolis-Gibbs method and comparison with linear locations*, Kluwer, Amsterdam, advances i edn.
- MacAyeal, D. R., Okal, E. A., Aster, R. C., & Bassis, J. N., 2008. Seismic and hydroacoustic tremor generated by colliding Icebergs, *Journal of Geophysical Research: Earth Surface*, **113**(3), 1–10.
- Malovrh, B. & Gandhi, F., 2005. Sensitivity of Helicopter Blade-Vortex Interaction Noise and Vibration to Interaction Parameters, *Journal of Aircraft*, **42**(3), 685–697.
- McNutt, S. R., 1992. Volcanic Tremor, *Encyclopedia of Earth System Science*, **4**, 417–425.
- Megies, T., Beyreuther, M., Barsch, R., Krischer, L., & Wassermann, J., 2011. ObsPy - what can it do for data centers and observatories?, *Annals of Geophysics*, **54**(1), 47–58.
- More, J. J., 1978. *The Levenberg-Marquardt algorithm: Implementation and theory*, vol. 630.
- Neuberg, J., Luckett, R., Baptie, B., & Olsen, K., 2000. Models of tremor and low-frequency earthquake swarms on Montserrat, *Journal of Volcanology and Geothermal Research*, **101**(1-2), 83–104.
- Nishie, S. & Akagi, M., 2013. Acoustic sound source tracking for a moving object using precise doppler-shift measurement, *Eusipco*.
- Oh, D. & Lee, J., 2014. Robust super-resolution TOA estimation against doppler shift for vehicle tracking, *IEEE Communications Letters*, **18**(5), 745–748.
- Rienstra, S. W. & Hirschberg, A., 2004. An introduction to acoustics, *Eindhoven University of Technology*, **18**(March), 19.
- Robinson Helicopter Company, 1992. R44 Pilot's Operating Handbook, Tech. rep.
- Soosalu, H., Einarsson, P., & Þorbjarnardóttir, B. S., 2005. Seismic activity related to the 2000 eruption of the Hekla volcano, Iceland, *Bulletin of Volcanology*, **68**(1), 21–36.
- Steel, C., 2009. Reconciling university teacher beliefs to create learning designs for LMS environments, *Australasian Journal of Educational Technology*, **25**(3), 399–420.
- Talandier, J., Hyvernaud, O., Reymond, D., & Okal, E. A., 2006. Hydroacoustic signals generated by parked and drifting icebergs in the Southern Indian and Pacific Oceans, *Geophysical Journal International*, **165**(3), 817–834.